photonics

MDPI

Article

Efficiency Dependence of Radiation-Assisted Ceramic Synthesis Based on Metal Oxides and Fluorides on Initial Powder Particle Sizes

Victor Lisitsyn [1,*], Elena Polisadova [1], Liudmila Lisitsyna [2], Aida Tulegenova [3,4], Igor Denisov [1] and Mikhail Golkovski [5]

[1] Department of Materials Science, Engineering School, National Research Tomsk Polytechnic University, 30, Lenin Ave., Tomsk 634050, Russia; elp@tpu.ru (E.P.); dip@tpu.ru (I.D.)
[2] Department of Physics, Chemistry and Theoretical Mechanics, Tomsk State University of Architecture and Building, 2, Solyanaya Sq., Tomsk 634003, Russia; lisitsyna@mail.ru
[3] Institute of Applied Science & Information Technology, 280, Baizakov Str., Almaty 050042, Kazakhstan; tulegenova.aida@gmail.com
[4] National Nanotechnology Laboratory of Open Type (NNLOT), Al-Farabi Kazakh National University, 71, Al-Farabi Ave., Almaty 050040, Kazakhstan
[5] Budker Institute of Nuclear Physics, SB RAS, 11, Lavrentiev Ave., Novosibirsk 630090, Russia; golkovski@mail.ru
* Correspondence: lisitsyn@tpu.ru; Tel.: +79-138242469

Abstract: The study is devoted to investigating the efficiency dependence of radiation-assisted ceramic synthesis based on metal oxides and fluorides on initial powder particle sizes. The synthesis was performed for 30 series of ceramic samples, including MgO, Al_2O_3, ZnO, ZrO_2, MgF_2, and complex compositions: cerium-activated yttrium-aluminum garnet ($Y_3Al_5O_{12}$), spinel $AlMgO_4$, and tungstate $MgWO_4$. The synthesis efficiency was evaluated on the mixture weight magnitude losses, morphology, and relative weight of the obtained ceramic samples. Based on the analysis of the synthesis results and measuring the particle distribution spectra of the initial materials, the criteria for selecting the initial materials were established, and possible explanations for the correlation between synthesis efficiency and the initial materials morphology were proposed.

Keywords: ceramics; spinel; radiation synthesis; efficiency; metal oxides

Citation: Lisitsyn, V.; Polisadova, E.; Lisitsyna, L.; Tulegenova, A.; Denisov, I.; Golkovski, M. Efficiency Dependence of Radiation-Assisted Ceramic Synthesis Based on Metal Oxides and Fluorides on Initial Powder Particle Sizes. *Photonics* **2023**, *10*, 1084. https://doi.org/10.3390/photonics10101084

Received: 9 August 2023
Revised: 18 September 2023
Accepted: 26 September 2023
Published: 27 September 2023

1. Introduction

The optical materials based on metal oxides and fluorides have found wide application as phosphors for LEDs [1,2], scintillators [3,4], and long-lasting afterglow light markers [5]. These materials are also used as temperature sensors [6] and transparent optical media [7]. Each application requires materials with different properties. There is a growing demand for the development of new materials with complex elemental composition and structure, possessing novel properties. The synthesis of refractory dielectric materials poses a challenging task. It involves not only high temperatures, but also the creation of new materials from simple starting compounds with significantly different melting points. Therefore, complex multi-step technological approaches are used for synthesis, creating conditions to promote elemental exchange among initial materials through the addition of additional substances and mechanical treatment.

Numerous research studies have been conducted aiming at the development and improvement of synthesis methods for materials based on refractory metal oxides and metal fluorides. In works [8–10], a brief description of the utilized synthesis methods and their comparison is presented.

The most widespread are thermal methods [11,12]. In the thermal synthesis method, the initial materials of good quality, usually in the form of fine-dispersed powders with a

specified stoichiometric composition, are thoroughly mixed and heated to temperatures below the melting point of the most easily melting component. Over an extended period, partial sintering and elemental exchange occur in the heated mixture. To accelerate the process of diffusional elemental exchange between particles of different composition in the mixture prior to heating, a flux, a substance with a melting temperature below the melting temperature (approximately 70%) of the most easily melting component of the mixture, is added. This achieves the replacement of solid-state diffusion processes with liquid-phase diffusion processes, which proceed at significantly higher rates. After cooling, the obtained ceramic is crushed into micrometer-sized particles. Subsequently, the resulting powder undergoes multiple high-temperature cyclic annealing steps (at approximately 80% of the melting temperature) over a period of 40–50 h to complete the formation of the desired phase and evaporation of the flux. Thus, the process of forming a new phase by thermal methods takes a considerable amount of time and might not completely eliminate all substances introduced during the synthesis. Nonetheless, this method is the most common, allowing the production of a high-quality final product with high reproducibility due to careful adherence to technological regulations.

There are also alternative synthesis methods [13–18], for instance, the arc plasma melting technique, where initial powders are ground in and pressed under high pressure. Arc plasma synthesis was conducted in the arc furnace. The material is melted in an inert argon gas environment. Polycrystalline materials with a transparent layer (shell) and a white core are obtained. The sol-gel method involves the chemical reactions of precursors to form the desired molecular composition. Subsequently, an extensive multi-step process is employed to eliminate excess elements, followed by multiple high-temperature cyclic annealing steps to complete the formation of particle structure and sizes. The synthesis process is challenging to control and time-consuming.

The possibility of synthesizing refractory dielectric materials using the combustion synthesis method, flame synthesis [19–21], is being studied. The prepared mixture for synthesis is blended with combustible materials and heated to the fuel ignition temperature. In the high-temperature flame of the combustible, the desired structure is formed. The synthesis process takes only a few minutes, which is the main advantage of the method. However, after synthesis, it is necessary to carry out purification of the obtained powder or ceramics from the remnants of the combustible material.

In recent years, much attention has been devoted to studying the possibility of synthesizing high-temperature resistant ceramics using the spark plasma sintering (SPS) method. Extremely high currents, resembling discharges in the material, are passed through the prepared mixture. This leads to rapid melting of the material and the formation of new phases. In order to increase the current flow, substances enhancing conductivity may be added to the mixture. The synthesis can be conducted at high pressure and in any atmosphere. The process can be completed within a few minutes, allowing for the potential production of transparent ceramics.

The impact of hard radiation fluxes during the synthesis process can facilitate the occurrence of essential solid-state reactions between medium elements, enhancing the efficiency of forming a new structure [22,23]. Upon exceeding certain threshold power levels of radiation flux in materials, a change in the nature of element exchange reactions between the medium particles may occur; reactions can be realized with the involvement of short-lived radiolysis products. Studies [24–26] have demonstrated that high-power hard radiation fluxes can be utilized for the synthesis of refractory dielectric materials with high efficiency.

The requirements for the properties of starting materials for the synthesis of new materials vary when different methods of forming new structures are employed. In thermal synthesis, the efficiency of synthesis (time, quality) is higher with smaller precursor particle sizes. Smaller particle sizes increase the likelihood of element exchange between particles. It is assumed that in radiation-assisted ceramic synthesis, the formation of new structures occurs in an electron-ion plasma created by a powerful stream of high-energy radiation.

Therefore, it is necessary to study the dependence of the results of radiation synthesis on the properties of the starting materials. In [27], while studying the dependence of radiation synthesis efficiency on the prehistory of the starting materials, a correlation between the synthesis outcome and the dispersed composition of the materials used for the synthesis was observed. The present study is dedicated to exploring the dependence of the efficiency of radiation-assisted synthesis of ceramics based on metal oxides and fluorides on the particle sizes of the initial powders.

2. Materials and Methods

The synthesis of materials was carried out by direct electron beam irradiation of the initial mixture of the specified composition using the ELV6 electron accelerator at the Budker Institute of Nuclear Physics, Siberian Branch of the Russian Academy of Sciences. The electron energy could vary in the range of 1.4–2.5 MeV, with a beam power of up to 90 kW. The beam, extracted through the system of differential pumping, had a Gaussian shape with a cross-sectional area of 1 cm^2 at the target surface. The electron accelerator, serving as a powerful source of hard radiation, ensures high energy conversion efficiency, and possesses a simple and easily controllable design.

The mixture of a given composition with a volume of 50 cm^3 was poured into a cavity of a massive copper crucible with a surface area of 10 × 5 cm^2. The crucible was positioned on a massive metal table below the exit aperture of an accelerator. A high-energy electron beam was scanned at a frequency of 50 Hz across the crucible in the transverse direction and moved relative to the scanning beam at a speed of 1 cm/s. The total duration of the electron beam exposure on the entire surface of the mixture was 10 s. The optimal values of electron beam flux densities for obtaining the desired materials were selected experimentally. For all materials investigated in this study, sufficient electron beam power densities for ceramic synthesis ranged from 13 to 25 kW/cm^2. The synthesis was realized solely using the energy of the radiation beam from the charge materials, without any addition of other facilitating materials, in a time less than "1 s".

A brief overview of the known dispersion information of the materials utilized in this study for investigations and analyses is presented in Table 1. The table provides the material's formula, along with either the name assigned by the manufacturer or, in parentheses, an arbitrary number assigned upon receipt. In parentheses, the batch number is provided, along with the powder's name.

Table 1. Characterization of powder particle sizes used for synthesis.

Initial Powders for Synthesis, Name	Type and Grain Sizes of Initial Substances
MgO (1)	powders 5 μm–200 μm
MgO (K12)	1 μm–10 μm
MgF_2 (1)	powders 5 μm–200 μm
MgF_2 (Aldrich)	Micro-sized powders
Al_2O_3 (K7)	1 μm–10 μm
Al_2O_3 (F800)	6.5 μm–9.5 μm
Al_2O_3 (nano)	1 nm–200 nm
Al_2O_3 (1)	0.5 μm–100 μm
Al_2O_3 (2)	Flour 0.1 μm–5 μm
Al_2O_3 (3)	5 μm–200 μm
Y_2O_3 ITO, B	10 μm–20 μm
ZnO	5 μm–200 μm
ZrO_2 (1)	microparticles
ZrO_2 (2)	microparticles

3. Results

For the synthesis of ceramics, powders of metal oxides and fluorides were chosen: MgO (2570 °C), Al_2O_3 (2044 °C), ZnO (1975 °C), ZrO_2 (2715 °C), MgF_2 (1263 °C). The selection of these materials for investigation was motivated by the following reasons. All

the listed powders are used in the production of optical and luminescent materials. Their properties can be altered through the introduction of activators. Furthermore, all these materials possess high melting points (indicated in parentheses). The synthesis of the oxide and fluoride powders is realized through different technological approaches and equipment. The obtained powders of metal oxides and fluorides from various manufacturers exhibit diverse dispersions. This factor is crucial for achieving the objectives of this study, namely, to elucidate the influence of dispersion on the efficiency of radiation synthesis. There is an opportunity to select powders with different dispersions for synthesis, even though manufacturers typically provide only general information about this. Substances with known particle size ranges and their distributions were chosen for synthesis to the extent possible. For synthesis, initial materials of different grades, ranging from extra pure and for synthesis, were used. The selection of the materials for ceramic synthesis was based on the authors' experience in synthesizing various variants of high-temperature optical ceramics.

During the synthesis process, one or a series of several samples could be formed in crucibles. Subsequently, in the tables and figures, the authors used the designated numbers of sample series formed in the same crucible during the synthesis experiment.

Examples of ceramic sample synthesis results are presented in Figures 1 and 2 as photographs of the samples in crucibles. This representation allows for visual comparison among the samples. For demonstration purposes, photographs of MgO and Al_2O_3, ZrO_2 samples are provided, synthesized from initial materials with different histories, as described in Table 1. The ceramics of each composition were synthesized under the same conditions of radiation treatment. Most synthesized materials have the form of a plate or a series of samples in a crucible with a dense solid surface and a porous structure inside. In Figure 2a,b, you can see continuous plates and series of separated samples (Figures 1 and 2c–e).

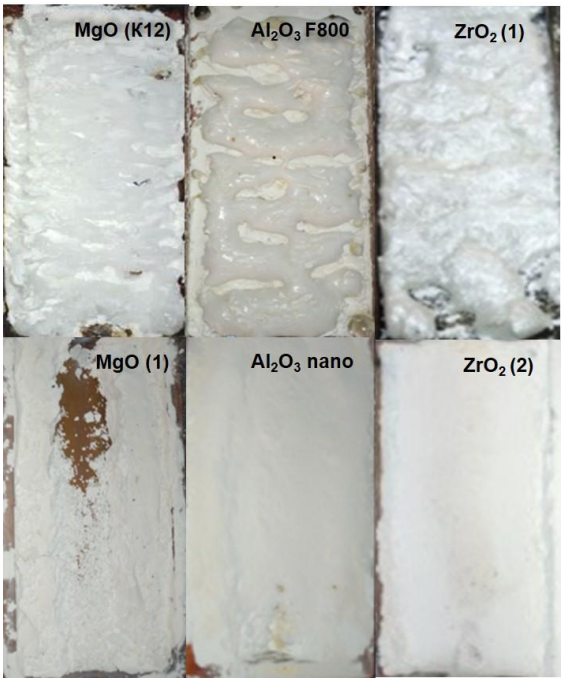

Figure 1. Photographs of samples in crucibles immediately after radiation treatment with 1.4 MeV electron flux with power density 26 kW/cm^2 of MgO mixture, 25 kW/cm^2-Al_2O_3, 25 kW/cm^2-ZrO_2 (1) microparticles, and 40 kW/cm^2-ZrO_2 (2) nanoparticles.

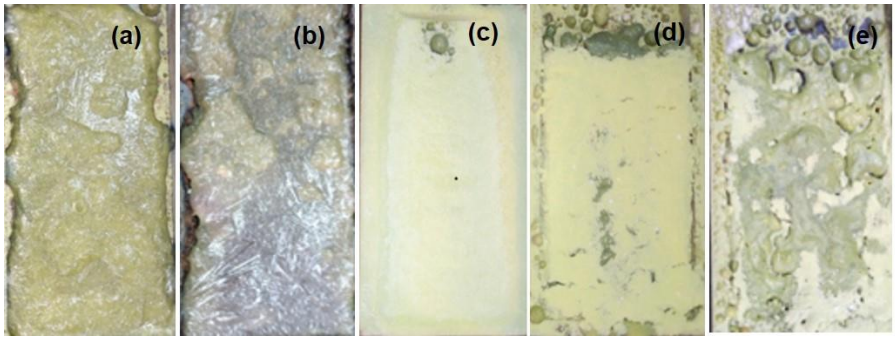

Figure 2. Radiation synthesis ceramics results of zinc tungstate $ZnWO_4$ ((**a**)-ZnO (1), (**b**)-ZnO (K9)) and magnesium tungstate $MgWO_4$ ((**c**)-MgO (1), (**d**)-MgO (K12), (**e**)-MgO (2)) based on a mixture of zinc oxide (ZnO), magnesium oxide (MgO), and tungsten oxide (WO_3) powders of varying dispersions after radiation treatment with a 1.4 MeV electron beam at a power density of 16 kW/cm^2.

Figure 1 shows example photographs of ceramic samples in crucibles synthesized from different precursor oxides, namely MgO, Al_2O_3, and ZrO_2, as described in Table 1. This presentation allows for visual comparison and examination of the samples among themselves.

A sample of MgO (K12) ceramics synthesized by electron flux treatment with an energy of 1.4 MeV and a power density of 26 kW/cm^2 appears as a solidified mass in the form of a plate within the entire crucible. The plate has a thickness of 2–4 mm. Beneath the plate lies a thin layer of mixture material, approximately 1–2 mm thick, which was not exposed to radiation and absorbed the entire electron flux in the upper layers of the mixture. The thickness of the mixture layer was adjusted to prevent the electron flux from reaching the copper crucible and contaminating the mixture with copper. Under the same radiation conditions, the synthesis of MgO (1) ceramic was not observed. The results of the radiation treatment of MgO (K12) and MgO (1) mixture materials were consistently reproducible across repeated experiments. The primary difference between the utilized powders is their particle sizes. The synthesis is effectively achieved using powders with particle sizes of 1–10 μm. MgO ceramics (1) were not formed from powders with particle sizes of 5–200 μm. As evidenced by the image, radiation treatment of the crucible with MgO (1) mixture material leads to significant spraying of a considerable portion of the mixture, with no evidence of ceramic formation. Thus, increasing the particle sizes of MgO to 5–200 μm complicates the synthesis process.

The same Figure 1 illustrates the difference in the efficiency of ceramic formation based on Al_2O_3. Synthesis is achieved when subjected to an electron flux with an energy of 1.4 MeV and a power density of 25 kW/cm^2 on Al_2O_3 (F800) mixture material with particle sizes of the powder ranging from 6.5–9.5 μm, but the same conditions did not result in the synthesis of Al_2O_3 nano mixture material. The particle sizes of Al_2O_3 nano powder range from 1–200 nm. From Al_2O_3 (F800) powder, a plate with a thickness of 2–4 mm is formed through radiation treatment within the entire crucible. Ceramic formation also occurs during the radiation treatment of Al_2O_3 (K7) mixture material with particle sizes of 1–10 μm. Beneath the ceramic plate, there is always a thin layer of mixture material, approximately 1–2 mm thick, which was not exposed to radiation. Following the radiation treatment of the crucible with Al_2O_3 nano powder, evidence of radiation impact remains, but no signs of ceramic formation are observed. Hence, reducing the particle sizes of Al_2O_3 to 1–200 nm also complicates the synthesis process.

Figure 1 also depicts the difference in the efficiency of ceramic formation based on ZrO_2. A solid ceramic plate is formed when exposed to an electron flux with an energy of 1.4 MeV and a power density of 25 kW/cm^2 on ZrO_2 (1) mixture material with micro-sized particles. However, the same conditions do not lead to synthesis when using ZrO_2 (2) mixture material with nano-sized particles. An attempt was made to achieve ceramic synthesis with higher power density, yet increasing the power density to 40 kW/cm^2 does

not lead to ceramic formation from ZrO_2 (2) mixture material. Thus, reducing the particle sizes of ZrO_2 to the nanoscale also complicates the synthesis process.

Similar dependencies of synthesis efficiency on particle sizes of utilized powders are evident for Y_2O_3 and MgF_2. It is noteworthy that radiation treatment allows for the synthesis of materials with varying properties, including melting temperatures. Furthermore, the synthesis of materials with significantly different properties is achieved under closely related radiation exposure conditions.

The dispersion of initial oxide and metal fluoride powders' properties can manifest in the synthesis efficiency of complex composition ceramics. Studies have been conducted on the synthesis of YAG ceramics ($Y_3Al_5O_{12}$: Ce, cerium-activated yttrium aluminum garnet) from Al_2O_3, Y_2O_3, Eu-activated alumina-magnesia spinel ($AlMgO_4$) from Al_2O_3, MgO, $MeWO_4$ tungstates from WO_3, MeO (Me: Mg, Zn). The synthesis was conducted using different combinations of the listed initial powders, as well as other unknown dispersions. It has been established that the synthesis outcome depends on the dispersion of the powders and their combinations.

Figure 2 provides images of crucibles with mixture materials for the synthesis of zinc and magnesium tungstates after radiation treatment using an electron flux with an energy of 1.4 MeV and a power density of 16 kW/cm^2. The mixture was prepared from tungsten oxide, zinc, and magnesium powders of stoichiometric composition. The same tungsten oxide (WO_3) was used for synthesis, with variations in the initial zinc and magnesium oxide powders. Zinc oxide (ZnO-1 and ZnO-2) and magnesium oxide (MgO-1, MgO-K12, and MgO-2) powders had different histories and dispersions.

When irradiating the mixture for the synthesis of zinc tungstate, plates of $ZnWO_4$ are formed as solidified molten masses. The plate morphology of $ZnWO_4$ is independent of the used powders of zinc oxide with varying precursors' history. However, the synthesis results of magnesium tungstate are dependent on the precursor oxide powders' history. When MgO-1 is employed to prepare the mixture, only a trace of irradiation effect remains after radiation treatment, and no ceramic is formed. Conversely, using MgO-K12 and MgO-2 powders, ceramic formation was observed after radiation treatment in the crucible.

From the presented results in Figure 2, it can be concluded that the probability of forming zinc and magnesium tungstate ceramics is not determined by the properties of tungstate oxide used, but solely by the properties of magnesium and zinc oxide powders. Similar synthesis results were obtained when studying the synthesis conditions of other ceramics such as yttrium aluminum garnet and spinel. It is noteworthy that the synthesis results (reproducibility, mass losses, synthesis efficiency) of a specific ceramic with selected initial materials do not differ by more than 10%. However, the range of these values, when using initial materials of different history for synthesizing complex composition ceramics, can vary from 0 to 100%.

The aforementioned research results concerning the synthesis outcome, particularly ceramic morphology, are difficult to explain solely by the presence of impurities. High-purity initial materials, including metal oxides and fluorides of extra pure grades and for synthesis, were used in this study. The presence of a small number of impurities is unlikely to significantly influence ceramic structure formation.

The influence of dispersion on radiation synthesis processes is entirely possible. Under the impact of a powerful flux of high-energy electrons, dielectric targets become charged. Particles of the mixture become charged, which could result in the mixture being sprayed. Evidently, the efficiency of spraying is dependent on the particle size of the mixture. In the synthesis of ceramics with complex compositions from mixed metal oxides, the unequal likelihood of particle spraying and violation of the stoichiometric mixture composition are possible.

Effective radiation synthesis under the influence of a powerful flux of electrons can be explained by the presence of ionization processes [25–27]. It is known that dielectric materials are sensitive to the effects of ionizing radiation. The decay of electron excitations into radicals is efficient in dielectric materials. It is presumed that in the field of intense

radiation, when the ionization density threshold in the dielectric mixture is exceeded, conditions for the formation of an electron-ion plasma are created. This plasma facilitates the efficient mixing of the mixture elements. The likelihood of the decay of electron excitations into structural defects or radicals is size-dependent when particle sizes are comparable to the range of self-excitations.

Experiments were conducted on the radiation synthesis of ceramics with different compositions from metal oxides and fluorides, followed by an analysis of synthesis efficiency. The mixture with a specified composition was subjected to radiation under optimal conditions. The term "optimal conditions" referred to those conditions under which the synthesis of a specific ceramic was realized using at least one of the initial compositions. It should be noted that all the ceramic samples listed in Table 2 below were synthesized at electron energies of 1.4 MeV and power density ranges of 15 to 27 kW/cm^2.

Table 2. Efficiency of conversion of the mixture placed in the crucible into ceramics.

Series Number	Composition of Mixture, Sample Code	Mixture Weight, g	Weight Loss %	Sample Weight, g	Yield Sample/Mixture
387	MgO (1)	21.3	3.8	1.1	5.3
484	MgO (K12)	29.3	0.7	9.8	33.5
492	Al_2O_3 (K7)	38.5	0.2	7.9	20.5
493	Al_2O_3 (nano)	43.3	17.2	1.9	4.5
458	BaF_2 (1)	48.7	1.5	21.5	44.2
518	BaF_2 (K14)	85.8	1.4	22.3	26
477	$MgAl_2O_4$, MgO (1), Al_2O_3 Er_2O_3 (0.5%)	43.9	13.5	20.2	45.1
480	$MgAl_2O_4$, MgO (2), Al_2O_3, Er_2O_3 (0.5%)	28.8	43.9	2.9	10.0
524	$MgAl_2O_4$, MgO (K1), Al_2O_3 (K7), Eu_2O_3 (0.5%)	35.2	0.3	12.1	34.4
449	MgF_2 (1)	39.4	3.0	10.1	25.6
515	MgF_2 (K13)	46.0	0.3	19.2	41.5
414	ZrO_2 (2)	41.7	55.9	0	0
90	ZrO_2 (1)	39.9	12.1	13.30	33.30
368	$Y_3Al_5O_{12}$: Ce, Al_2O_3 (F800), Y_2O_3, Ce_2O_3 (0.5%)	39.9	0.2	14.7	36.8
530	Y_3 Al_5O_{12}: Ce, Al_2O_3 (K7), Y_2O_3, Ce_2O_3 (0.5%)	60.4	0.46	58.4	97
468	ZnO (1)	25.8	2.4	12.4	48.1
498	ZnO (K9)	42.9	2.6	18.5	43.2
443	$MgWO_4$, MgO (1), WO_3 (K12)	44.48	27.59	4.82	10.8
447	$MgWO_4$, MgO (11), WO_3 (K12)	69.89	13.76	48.56	69.5
346	$MgWO_4$, MgO (2), WO_3 (K12)	73.29	33.23	40.06	45.3
510	$ZnWO_4$, ZnO (K9), WO_3 (K12)	94.2	1.29	86.87	95.2

In Table 2, information is presented regarding the mass loss of the mixture in the crucible and the efficiency of its conversion into ceramics. The efficiency of synthesis, as indicated in Table 2, is defined as the ratio of the mass of the resulting ceramic samples to the mass of the mixture before synthesis. It should be noted that the synthesis yield is not directly related to the mass of the obtained ceramic samples. Following synthesis, a portion of the mixture that did not participate in the reactions remains at the bottom of the crucible. This is done intentionally, as the thickness of the mixture layer needs to exceed the penetration depth of the electrons used in the synthesis. The information about mass losses provides insight only into the quantity of the initial mixture disappearing from the crucible

under the influence of the electron flux. Therefore, the synthesis yield values should be considered approximate. Nevertheless, they provide a good representation of the synthesis efficiency for various materials and its dependence on the properties of the initial materials and the conditions of the radiation treatment.

As inferred from the presented results in Table 2, there is a significant variability in the values of reaction yield and mass losses. For instance, the reaction yields of synthesized ceramics such as MgO (1), Al_2O_3 (nano), and ZrO_2 (2) range from 0% to 5%. Meanwhile, under closely related radiation exposure modes, the reaction yields of ceramics like MgO (K12) are 99.5%; Al_2O_3 (K7) are 93%, 94%, and 95%; ZrO_2 (1) is 33%; MgF_2 (K13) is 41%; and BaF_2 (1) is 44%. From the available information, these two groups of materials differ based on the dispersion of the initial substances used for synthesis.

Similar conclusions can be drawn for ceramics of complex compositions. Table 2 presents the measurement results of the reaction yield and mass losses for ceramics of yttrium aluminum garnet, alumina-magnesia spinel, and tungstates, produced from materials of varying prehistories. The reaction yields for alumina-magnesia spinel range from 10% to 45%, whereas for tungstates, they vary from 10.8% to 69%. For the well-studied yttrium aluminum garnet, the reaction yield can reach up to 97%.

4. Discussion

The presented research results lead to the conclusion that the processes and outcomes of the synthesis of the investigated ceramics depend on the particle sizes of the initial materials' powders. However, establishing quantitative correlations is still not feasible. The reason is that the information on the average particle sizes or size ranges is explicitly insufficient for understanding the influence of particle sizes on the synthesis processes occurring in the radiation field. Evidently, the particle morphology can also influence the ceramic synthesis process. To develop a better understanding of the impact of the characteristics of the initial materials on the radiation synthesis of ceramics, studies on the particle morphology of aluminum oxide powders with different histories were conducted using optical microscopy with the μVizo optical microscope (LOMO). Figure 3 illustrates the photographs of Al_2O_3 powders, F800 grade (Figure 3b), and nanopowders (Figure 3a) taken with the μVizo optical microscope (LOMO). A distinct difference in the powder morphology is evident. The nanoparticles of the nanopowder exhibit a non-crystalline form appearance, characteristic of conglomerated nanoparticles. The particles of the F800 powder appear as fragmented crystals with distinct cleavages. The sizes of conglomerated nanoparticles and microcrystals are comparable.

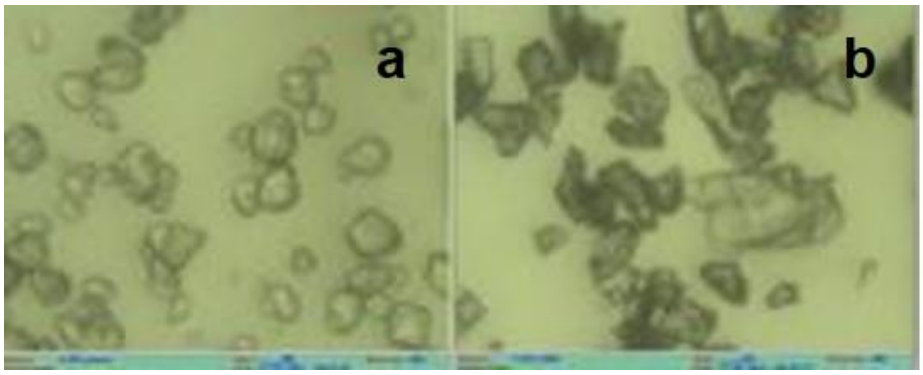

Figure 3. Image of Al_2O_3 powders of grade F800 (**a**) and nano-oxide (**b**) at a 100× zoom.

The dispersion analysis of the powders used for the synthesis of the initial precursors in order to obtain YAG ceramic samples was conducted using the laser diffraction method with the Shimadzu SALD-7101 Laser Particle Size Analyzer. Below, we will examine the results of the powder dispersion analysis and its potential impact, using the example of YAG ceramic synthesis.

Six types of alumina oxide powders were employed for the synthesis of YAG ceramics, the details of which are presented in Tables 1 and 2: Al_2O_3 (K7), Al_2O_3 (F800), Al_2O_3 (nano), Al_2O_3 (1), Al_2O_3 (2), and Al_2O_3 (3). All powders exhibited a wide spectra of particle distribution in terms of volume and size. In the case of Al_2O_3 (K7), the particle volume distribution primarily ranged between 0.01–0.4 µm and 3–12 µm. Al_2O_3 (F800) ranged from 4–15 µm, Al_2O_3 (nano) from 0.4–1.5 µm and 10–150 µm, Al_2O_3 (1) from 10–60 µm, Al_2O_3 (2) from 0.1–0.4 µm and 1–40 µm, and Al_2O_3 (3) from 10–200 µm. It is worth noting that in the case of Al_2O_3 (nano), large particles were conglomerates of nanoparticles, necessitating a distinct consideration of processes involving these powders. In terms of particle quantity distribution, Al_2O_3 (K7) primarily ranged from 0.01–0.05 µm and much smaller in 1–10 µm, Al_2O_3 (F800) from 0.4–1.0 µm and 2–8 µm, Al_2O_3 (nano) from 0.4–2.0 µm, Al_2O_3 (1) from 2–5 µm and 10–60 µm, Al_2O_3 (2) from 0.05–2 µm and less in 1–40 µm, and Al_2O_3 (3) from 0.4–2 µm. Across all variants of the investigated Al_2O_3 powders with varying histories, two distinct particle groups emerged: fine particles, ranging from 0.01–3 µm, and larger particles, ranging from 3 to 300 µm. The ratio between the volumes of fine and large particles, along with the quantity of each, exhibited significant variation among the powders with different measured dispersions. From the distribution spectra, it is evident that the quantity of fine particles in the total volume did not exceed 1–5%. Clearly, the synthesis outcome is primarily influenced by the volume of particles within the chosen range rather than the particle quantity.

As an example, Figure 4 depicts the particle size distribution of Al_2O_3 (K7) and Y_2O_3 powders in two representations: volume dependence (left) and particle quantity dependence on particle size (right).

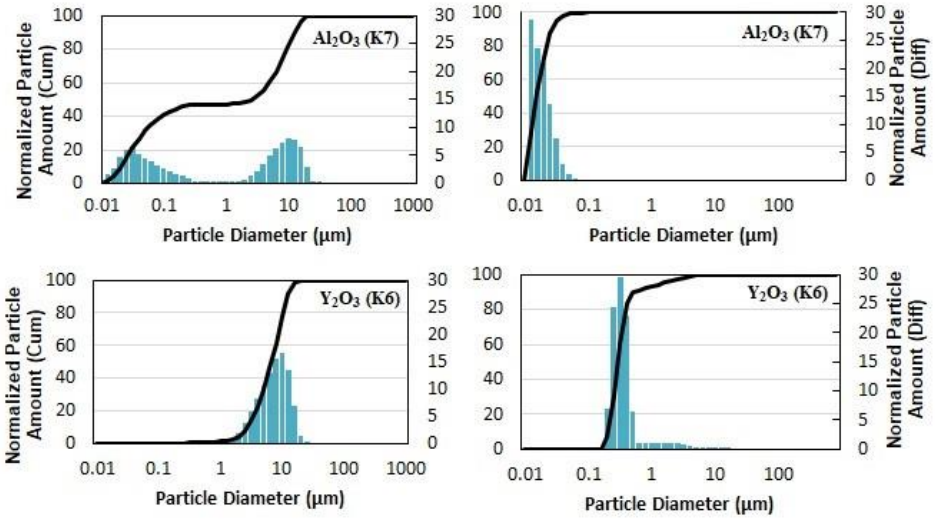

Figure 4. Particle distribution in aluminum oxide (Al_2O_3) and yttrium oxide (Y_2O_3) powders used for radiation-assisted ceramic synthesis by volume (**left column**) and by quantity (**right column**).

The synthesis of YAG ceramics from these powders occurs with high efficiency. These powders exhibit an overlap of distribution spectra within the range of 3–12 µm.

For the pairs Al_2O_3 (nano), Al_2O_3 (1), Al_2O_3 (3), and Y_2O_3, the synthesis efficiency is significantly lower. In these pairs, the overlap of particle size distribution spectra is minor.

In the case of a substantial difference in particle sizes between aluminum and yttrium oxides, a local deviation from the stoichiometric elemental composition of the mixture occurs. During the short radiation exposure of each elemental volume of the mixture, less than 2 ms under the applied radiation treatment conditions, and with radical lifetimes of less than 1 µs, averaging the distribution of radiolysis products in the volume becomes impossible. This fact evidently accounts for the low efficiency of YAG ceramic synthesis from the mixture prepared from the mentioned pairs.

The low efficiency of radiation synthesis of ceramics from nanoparticles might also be attributed to the fact that the electron excitations created within nanoparticles predominantly decay at the surface without generating radicals.

5. Conclusions

The radiation-assisted rapid synthesis of refractory ceramic optical materials has demonstrated its effectiveness. The derived regularities indicate that the combination of ceramic formation processes through direct exposure to a high-energy electron flux differs from those occurring during thermal synthesis. To assess the efficiency of converting excitation energy into luminescence in light-emitting diodes (LEDs), several LEDs were manufactured using ceramic fragments of phosphors obtained from two specialized factories. Light output measurements of the LEDs were also conducted at these facilities. It was demonstrated that the light output of the manufactured LEDs amounts to 80% of the light output of the LEDs produced by the factories in series.

The efficiency of radiation synthesis of ceramics based on metal oxides and fluorides from initial powders depends on particle sizes and their morphology. The optimal particle sizes for ceramic sample synthesis under the utilized radiation exposure modes (power density) range from 1 to 15 μm, with the distribution peak around 5–10 μm, which is consistent for all utilized initial components. For smaller particle sizes, it is likely that electronic excitations decay on the particle's surface without generating radicals. The synthesis efficiency is higher for powders with a crystalline structure. With larger particle sizes, the likelihood of radicals (short-lived radiation defects) escaping beyond the particle boundary, forming an electron-ion plasma, diminishes.

When synthesizing ceramics with complex elemental compositions using a combination of initial material powders, attention must be paid to the potential mutual influence of their dispersions on the outcome. In cases where there is a significant difference in particle sizes, local areas with non-stoichiometric compositions may form. This effect is crucial in radiation synthesis, where ceramic formation occurs within timescales shorter than 2 ms. Within the brief radiation exposure time of each elemental volume of the initial material, less than 2 ms under the employed radiation treatment conditions, and considering the radicals' lifespan of less than 1 μs, averaging the distribution of radiolysis products within the volume becomes unfeasible.

Author Contributions: Conceptualization, V.L. and L.L.; methodology, M.G.; software, E.P.; validation, L.L., I.D. and M.G.; formal analysis, V.L.; investigation, V.L.; resources, E.P.; data curation, L.L.; writing—original draft preparation, V.L.; writing—review and editing, A.T.; visualization, L.L.; supervision, V.L.; project administration, V.L.; funding acquisition, E.P. All authors have read and agreed to the published version of the manuscript.

Funding: This research was funded by the Russian Science Foundation of the Russian Federation. (Grant No. 23-73-00108).

Institutional Review Board Statement: Not applicable.

Informed Consent Statement: Not applicable.

Data Availability Statement: The data presented in this study are available on request from the corresponding author.

Acknowledgments: In this work, for the analysis of powder dispersibility, we used the equipment of the CCU NMNT TPU, supported by the project of the Ministry of Education and Science of Russia No. 075-15-2021-710.

Conflicts of Interest: The authors declare no conflict of interest.

References

1. Liu, X.; Qian, X.; Zheng, P.; Chen, X.; Feng, Y.; Shi, Y.; Zou, J.; Xie, R.; Li, J. Composition and Structure Design of Three-Layered Composite Phosphors for High Color Rendering Chip-on-Board Light-Emitting Diode Devices. *J. Adv. Ceram.* **2021**, *10*, 729–740. [CrossRef]
2. Xia, Z.; Meijerink, A. Ce^{3+}-Doped Garnet Phosphors: Composition Modification, Luminescence Properties and Applications. *Chem. Soc. Rev.* **2017**, *46*, 275–299. [CrossRef] [PubMed]
3. Li, J.; Sahi, S.; Groza, M.; Pan, Y.; Burger, A.; Kenarangui, R.; Chen, W. Optical and Scintillation Properties of Ce^{3+}-Doped LuAG and YAG Transparent Ceramics: A Comparative Study. *J. Am. Ceram. Soc.* **2017**, *100*, 150–156. [CrossRef]
4. Lecoq, P. Development of New Scintillators for Medical Applications. *Nucl. Instrum. Methods Phys. Res. Sect. A Accel. Spectrometers Detect. Assoc. Equip.* **2016**, *809*, 130–139. [CrossRef]
5. Sharma, S.K.; James, J.; Gupta, S.K.; Hussain, S. UV-A,B,C Emitting Persistent Luminescent Materials. *Materials* **2022**, *16*, 236. [CrossRef] [PubMed]
6. Sun, H.; Gao, Q.; Wang, A.; Liu, Y.; Wang, X.; Liu, F. Ultraviolet-B Persistent Luminescence and Thermoluminescence of Bismuth Ion Doped Garnet Phosphors. *Opt. Mater. Express* **2020**, *10*, 1296–1302. [CrossRef]
7. Xiao, Z.; Yu, S.; Li, Y.; Ruan, S.; Kong, L.B.; Huang, Q.; Huang, Z.; Zhou, K.; Su, H.; Yao, Z.; et al. Materials Development and Potential Applications of Transparent Ceramics: A Review. *Mater. Sci. Eng. R Rep.* **2020**, *139*, 100518. [CrossRef]
8. Pan, Y.; Wu, M.; Su, Q. Comparative Investigation on Synthesis and Photoluminescence of YAG:Ce Phosphor. *Mater. Sci. Eng. B* **2004**, *106*, 251. [CrossRef]
9. Smet, P.F.; Parmentier, A.B.; Poelman, D. Selecting Conversion Phosphors for White Light-Emitting Diodes. *J. Electrochem. Soc.* **2011**, *158*, R37. [CrossRef]
10. Ye, S.; Xiao, F.; Pan, Y.X.; Ma, Y.Y.; Zhang, Q.Y. Phosphors in Phosphor-Converted White Light-Emitting Diodes: Recent Advances in Materials, Techniques and Properties. *Mater. Sci. Eng. R Rep.* **2010**, *71*, 1–34. [CrossRef]
11. Wang, X.; Li, J.; Shen, Q.; Shi, P. Flux-Grown $Y_3Al_5O_{12}$:Ce^{3+} Phosphors with Improved Crystallinity and Dispersibility. *Ceram. Int.* **2014**, *40*, 15313–15317. [CrossRef]
12. Yang, Y.; Wang, X.; Liu, B.; Zhang, Y.; Lv, X.; Li, J.; Wei, L.; Yu, H.; Hu, Y.; Zhang, H. Molten Salt Synthesis and Luminescence of Dy^{3+}-doped $Y_3Al_5O_{12}$ Phosphors. *Luminescence* **2020**, *35*, 580–585. [CrossRef] [PubMed]
13. Pereira, P.F.S.; Matos, M.G.; Ávila, L.R.; Nassor, E.C.O.; Cestari, A.; Ciuffi, K.J.; Calefi, P.S.; Nassar, E.J. Red, Green and Blue (RGB) Emission Doped $Y_3Al_5O_{12}$ (YAG) Phosphors Prepared by Non-Hydrolytic Sol–Gel Route. *J. Lumin.* **2010**, *130*, 488–493. [CrossRef]
14. Abdullin, K.A.; Kemel'bekova, A.E.; Lisitsyn, V.M.; Mukhamedshina, D.M.; Nemkaeva, R.R.; Tulegenova, A.T. Aerosol Synthesis of Highly Dispersed $Y_3Al_5O_{12}$:Ce^{3+} Phosphor with Intense Photoluminescence. *Phys. Solid State* **2019**, *61*, 1840–1845. [CrossRef]
15. Grazenaite, E.; Garskaite, E.; Stankeviciute, Z.; Raudonyte-Svirbutaviciene, E.; Zarkov, A.; Kareiva, A. Ga-Substituted Cobalt-Chromium Spinels as Ceramic Pigments Produced by Sol–Gel Synthesis. *Crystals* **2020**, *10*, 1078. [CrossRef]
16. Dai, P.; Ji, C.; Shen, L.; Qian, Q.; Guo, G.; Zhang, X.; Bao, N. Photoluminescence Properties of YAG:Ce^{3+},Pr^{3+} Nano-Sized Phosphors Synthesized by a Modified Co-Precipitation Method. *J. Rare Earths* **2017**, *35*, 341–346. [CrossRef]
17. Kruk, A.; Jany, B.; Owczarczyk, K.; Madej, D. On the Possibility of Using Arc Plasma Melting Technique in Preparation of Transparent Yttria Ceramics. *Opt. Appl.* **2019**, *49*, 355–364. [CrossRef]
18. Kruk, A. Fabrication of MgO High Transparent Ceramics by Arc Plasma Synthesis. *Opt. Mater.* **2018**, *84*, 360–366. [CrossRef]
19. Serrano-Bayona, R.; Chu, C.; Liu, P.; Roberts, W.L. Flame Synthesis of Carbon and Metal-Oxide Nanoparticles: Flame Types, Effects of Combustion Parameters on Properties and Measurement Methods. *Materials* **2023**, *16*, 1192. [CrossRef]
20. Huczko, A.; Kurcz, M.; Baranowski, P.; Bystrzejewski, M.; Bhattarai, A.; Dyjak, S.; Bhatta, R.; Pokhrel, B.; Kafle, B.P. Fast Combustion Synthesis and Characterization of YAG:Ce^{3+} Garnet Nanopowders: Fast Combustion Synthesis of YAG:Ce^{3+} Garnet Nanopowders. *Phys. Status Solidi B* **2013**, *250*, 2702–2708. [CrossRef]
21. Ohyama, J.; Zhu, C.; Saito, G.; Haga, M.; Nomura, T.; Sakaguchi, N.; Akiyama, T. Combustion Synthesis of YAG:Ce Phosphors via the Thermite Reaction of Aluminum. *J. Rare Earths* **2018**, *36*, 248–256. [CrossRef]
22. Le Godec, Y.; Le Floch, S. Recent Developments of High-Pressure Spark Plasma Sintering: An Overview of Current Applications, Challenges and Future Directions. *Materials* **2023**, *16*, 997. [CrossRef]
23. Boldyrev, V.V.; Zakharov, Y.A.; Konyshev, V.P.; Pinaevskaya, E.N.; Boldyreva, A. On Kinetic Factors Which Determine Specific Mechano-Chemical Processes in Inorganic Systems. *Kinet. Katal.* **1972**, *13*, 1411–1421.
24. Lisitsyn, V.M.; Golkovsky, M.G.; Musakhanov, D.A.; Tulegenova, A.T.; Abdullin, K.A.; Aitzhanov, M.B. YAG Based Phosphors, Synthesized in a Field of Radiation. *J. Phys. Conf. Ser.* **2018**, *1115*, 52007. [CrossRef]
25. Lisitsyn, V.; Tulegenova, A.; Kaneva, E.; Mussakhanov, D.; Gritsenko, B. Express Synthesis of YAG:Ce Ceramics in the High-Energy Electrons Flow Field. *Materials* **2023**, *16*, 1057. [CrossRef] [PubMed]

26. Lisitsyn, V.M.; Musakhanov, D.A.; Korzhneva, T.G.; Strelkova, A.V.; Lisitsyna, L.A.; Golkovsky, M.G.; Zhunusbekov, A.M.; Karipbaev, J.T.; Kozlovsky, A.L. Synthesis and Characterization of Ceramics $Ba_xMg_{(2-x)}F_4$ Activated by Tungsten. *Glass Phys. Chem.* **2023**, *49*, 288–292. [CrossRef]
27. Lisitsyn, V.M.; Karipbayev, Z.T.; Zhilgildinov, Z.S.; Zhunusbekov, A.M.; Tulegenova, A.T.; Golkovski, M.G. Effect of Precursor Prehistory on the Efficiency of Radiation-Assisted Synthesis and Luminescence of YAG:Ce Ceramics. *Photonics* **2023**, *10*, 494. [CrossRef]